ANALYSIS OF THE EVOLUTION AND DEFORMATION OF PORE MORPHOLOGY DURING COMPRESSION

Li Wei[1], Tingan Zhang[2], Yuan Fang[1] and Yunan Tian[1]

[1]Department of Materials Science and Engineering, Shenyang Ligong University, Liaoning, Shenyang, 110159, China;
[2]School of Materials and Metallurgy, Northeastern University, Liaoning, Shenyang, 110819, China;

Keywords: X-ray tomography, aluminum foam, pore morphology, compression, structure evolution

Abstract

In this paper, the X-ray tomography is used to observe the evolution of pore morphology during the compression of aluminum foam. The pore morphological tomography images for every cross-section were obtained, and the evolution regularity was analyzed in different compression stages. The results of the research work show that the pore morphology evolution is closely related with the cell wall structure. There are non-uniform pore structure and cell wall defects generated in the preparation process of aluminum foams. Foam Al-Si alloy presents brittle fracture in the process of compression as for the reason of brittleness in its base metal. This crack first appears in the area of the cell wall with defects. As the pressure increases, the crack continues to expand and deepen with fractures appearing in some cell walls, and eventually forming a fracture zone; finally, the entire sample is compacted and crushed. Foam magnesium alloy presents good ductility in the process of compression. Bending deformation of the cell wall occurs, and expands to the central area until the entire sample is compacted.

Introduction

Foam aluminum materials as a new type of material with structural-function integration has been widely recognized and has attracted great attention due to its various excellent physical, mechanical [1-3] and chemical properties [4-6]. Much research has been carried out on its preparations, performances and applications [7-8]. Foam aluminum materials, however, are still brand new without the mature technologies that have the defect of dispersibility. Mukhrjee et al. [9] pointed out that not only the properties of basis material, but factors of the pore morphology, size distribution, pore size and porosity etc. has great effects on aluminum foam performances. In the meanwhile, ZHANG et al. and Tabibian et al. [10-11] showed that the characteristics of the pore structure determine the compression and energy absorption behavior on one of the most representative researches. Currently, Seitzberger et al. works [12] that focus on the studies of dynamic and static mechanical properties on lab basis, the regular honeycomb or cube structure of the bubbles are also studied by De Giorgi et al. and Yu et al. [13-14] with theoretical deduction and numerical simulation for the pore structure that cannot truly demonstrate the highly complexity and disorder. The real evolution process of pore morphology has rarely been reported, especially for the pore structure testing of porous metal material by Saadatfar et al. and Yang et al. [15-16] with electronic computer X-ray tomography technique.

During the compression process, the changing of pore structure is very complex. One cannot accurately describe the changing by adopting regular statistical approach to studying a certain cross section [17]. If the morphological evolution is carried out for the entire section of pores, the statistical distribution rule of the main micro structural geometric parameters is obtained, so that the evolement rule can be accurately described [18]. Therefore, in this paper, the morphologic changes for each cross section are obtained by electronic computer X-ray tomography technique during compression process, analyzing the evolement rule of pore morphology on each compression stage, so that it can provide the evidence to study the relationship between the structural feature and the performance.

Materials and experimental procedure

Sample preparation

The mechanical properties of the matrix is one of the main factors that determines the mechanical properties of the aluminum foam, the matrix materials which are widely used to prepare aluminum foam are currently Al-Si alloy and Al-Mg alloy. In the compression energy absorption performance, closed-cell aluminum foam prepared by melt foam and powder metallurgy method showed a more prominent feature, so the research in this paper is focused on these kinds of materials. Pore size distribution is another important factor that determines the compression performance of aluminum foam; two kinds of aluminum materials with different porosity and size distribution were selected for the study in the experiment. Al-Si alloy foam is named **Foam I**, magnesium alloy foam is named **Foam II**. Al-Si alloy foam was prepared by 'Alporas' method. Calcium metal is added to an aluminum melt at 680℃. The melt is stirred for several minutes during which its viscosity continuously increases owing to the formation of calcium oxide (CaO), calcium–aluminum oxide ($CaAl_2O_4$) or perhaps even Al4Ca intermetallic that thickens the liquid metal. For the actual foam production, usually 1.5–3 wt% Ca is added. After the viscosity has reached the desired value, titanium hydride (TiH_2) is added (typically 1.6wt %), which serves as a blowing agent by releasing hydrogen gas in the hot viscous liquid. The melt soon starts to expand slowly and gradually fills the foaming vessel. The foaming takes place at constant pressure. After cooling down the vessel below the melting point of the alloy the liquid foam turns into solid aluminum foam and can be taken out of the mould for further processing. The entire foaming process can take 15 *min* for a typical large batch.

Al-Mg alloy foam was prepared using the powder metallurgical (PM) production method. The production process begins with the mixing of metal powders – elementary metals, alloys or powder blends – with a foaming agent, after which the mix is compacted to yield a dense, semi-finished product. Heat treatment at a

temperature near the melting point of the matrix material is the next step. During this process the foaming agent, which is homogeneously distributed within the dense metallic matrix, decomposes. The released gas forces the compacted PM material to expand into its highly porous structure. The samples were sectioned by electro-discharge machining to cuboid shapes of $40mm \times 40mm \times 16mm$ (**Foam I**) and $35mm \times 32mm \times 13mm$ (**Foam II**), and the outer skins of the foams were removed.

Experimental procedure

Compressive strength tests were carried out on the 810 Material Test System in the Mechanics of Materials Laboratory of University of Leicester. The samples were sectioned by electro-discharge machining, and the outer skins of the foams were removed. Samples in cuboid shapes with different density and pore structure were electro-discharge machined to $40mm \times 40mm \times 16mm$ pieces from the foamed plates. Before compression, the axial force and displacement should to be adjusted to zero upon the sample touching both upper and lower indenters. The velocity of compression bar is set to 2 mm/min, and can be stopped according to the amount predetermined. Finally, the sample will be unloaded with the velocity of 0.1 mm/sec. The pore size and the density of the foam can be controlled by the heating temperature and processing time.

Micro-structural and size distribution examination was performed using X-TEK XT H 225 X-ray computed tomography (X-ray CT) manufactured by Nikon, with 240 kV microfocus X-ray source, which can rotate the sample through 360° for one interval of 1° for one image. The voltage and current are set around 150kV and $130\mu A$, respectively. Three-dimensional (3D) reconstruction of the data was performed using the commercial software Octopus. After reconstruction, the commercial software VGStudioMax 1.2.1 was used to extract 2D and 3D sections of the foam. The cell size distribution of the sample was represented as an equivalent diameter of a circle with the same area, and then was described using the professional image analysis software ImagePro Plus 6.0 (IPP6.0). For the compressed samples the cell size analysis was performed only for the first layer of the X-ray CT 2D image.

Image analysis method

There are many defects in the aluminum foam, such as congenital absence of the cell wall, that will cause the image recognition software used to automatically identify these cells into a large cell and cause statistical errors, The missing walls will therefore be repaired using a brush before counting. The discrete cells are numbered sequentially as 1, 2, 3, ….., i, … using IPP6.0 software, and then cell numbers and sizes are counted for every image. In order to comfortably describe the experiment results, a uniform coordinate is established for the images of samples in every compression stage, shown in **Figure 1**.

Pressure load direction is opposite to the z-axis direction, the section parallel to XOZ section is the cross-section. Different sections along the y-axis direction are analyzed, y represents the relative distance of at $y=0$.
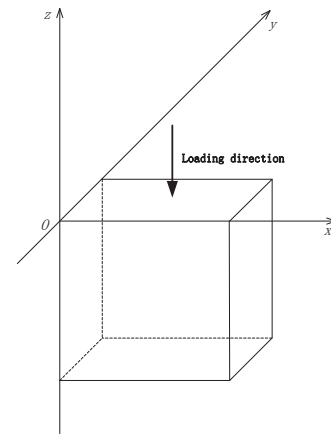
Figure 1 Schematic diagram coordinate for 3-D reconstruction of the specimen

Results and discussion

Basic features of the sample

The basic features of Al-Si alloy foam Al-Mg alloy foam obtained by X-ray CT are shown in **Table 1**.

Table 1 Detail of the samples based on the X-ray tomography image

Sample		Foam I	Foam II
Size(mm)		40(high) ×40(length) ×16(width)	35(high) ×32(length) ×13(width)
Density (g/cm^3)		0.595	0.450
Porosity (%)		78.00	83.50
Diameter (mm)	Min	0.09	0.10
	Max	7.75	5.26
	Mean	2.44	1.23
Area (mm^2)	Min	0.0016	0.0021
	Max	48.0049	24.0198
	Mean	8.22	3.0

Cell size distribution

From the cell size distribution in different compression stages shown in **Figure 2**, it can be seen that the size ranges widely before compression. In **Foam I**, the cells less than 0.5mm account to 20.18%, the cells between 5.5-6.0mm account to 0.8%, and the cells between 7.0-8.0mm account for 2.63%. During compression (compressed 0-18.43%), the cells in middle and large size are compressed first, the percentage of cells in small size increases; the number of cells smaller than 0.5mm increases to 39.62%, the cells between 5.5-6.0mm account 2.83%, and there are no cells larger than 6.0mm. With the increase in the amount of compression, some of the cell walls are broken or compacted, the percentage of small size cells decreased, but it still accounts for the majority of size distribution. When the compression increases to 43.80%, the number of cells less than 0.5mm accounts 27.78%, the cells between 4-4.5mm are only about 5.56%, the cells greater than 4.5mm are no longer present. The size distribution of cells in **Foam II** is between 0.5-6.0mm. The cells size less than 0.5mm account to 57.6%, and the cells greater than 5.5mm account to 1%. As the compression increases, the cells in large size become smaller, the cells in small size are gradually compacted. When the

compression amount increases to 20%, the cells number with smaller than 0.5*mm* increases to 60.98%, and the cells with larger than 5.5*mm* decreases to 0.8%. When the compression is increased to 60%, the number of the cells smaller than 0.5*mm* increases to 66.6%, the number of the cells in size between 3.5-4.0*mm* is about 0.4%, and the cells larger than 4.0*mm* are no longer present.

Foam I

Foam II
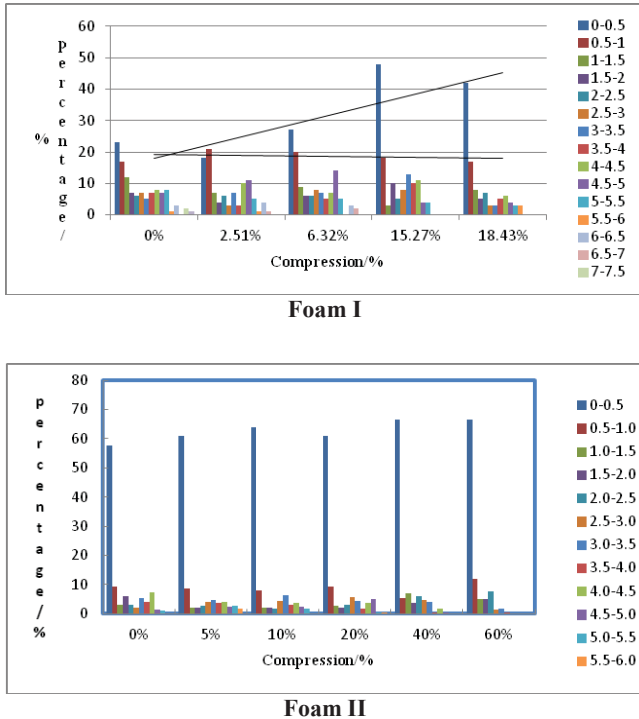
Figure 2 Cell size distribution in difference compression stage

Cell diameter, area and porosity distribution

The average diameter, average area and porosity are shown in **Figure 3** in the different compression stages. It can be seen from the figure that, as the compression increases, the average pore diameter becomes smaller. For **Foam I**, during the period of compression between 0-2.51%, there is a small increase in average diameter and area of cells. When the compression is greater than 2.51%, it decreases linearly, and the slope is -0.049, it reaches to its minimum when the compression is 39.7%. It shows that the change in diameter and porosity of **Foam I** is very obvious during compression. Combined with the images of X-ray CT, it can be seen that not only do some cells become smaller during compression, but some cell walls also become broken and compacted, which results in the rapid decrease in the average diameter of the cells.

For **Foam II**, as the compression increases, the cell sizes are reduced as well, but much more smoothly than that of **Foam I**, even more, when the compression is 10% -20%, the changing rate is nearly zero (the slope is nearly zero), and when the compression is greater than 20%, the slope is about -0.015%.

From the X-ray CT images, it can be seen that, when the compression is small, only some of the upper portion of the sample cell walls bending deformation occurs, the number of the cells is reduced, but the cells do not disappear.
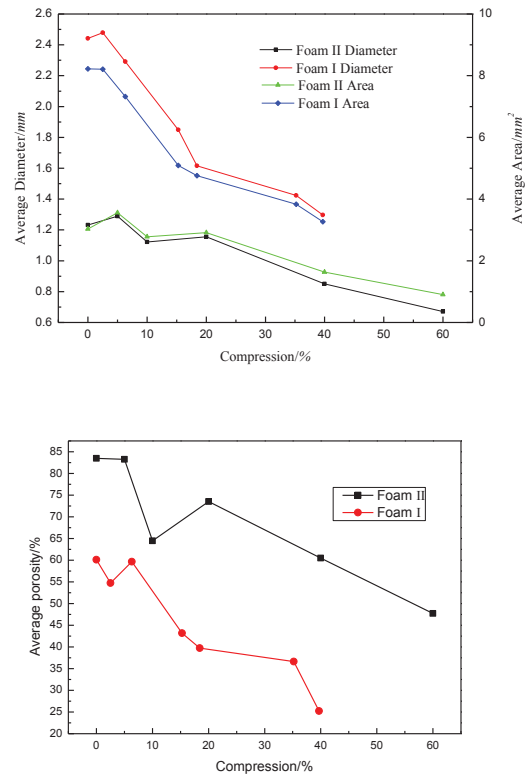
Figure 3 Diameter, area and porosity of cell in different compression stage

Pore morphology evolution

The sequence of fracture events during compression of the samples of **Foam I** and **Foam II** is shown in **Figures 4** and **5**. For the sample of **Foam I**, there are some defects in the cell walls. Several broken cell walls can be seen in the region highlighted using a red circle in original micrograph image (**Figure 3a).** Some of cracks appeared on the cell walls when the sample was compressed by 2.51% compression. Further cracks occurred in this region and some of cell wall fractures, and a fracture zone formed when the compression was 6.32%. At the same time, cracks were generated in another region that had pre-existing defects in the cell walls. As the compression proceeded (15.27% compression), some of cell walls began to crack. When the compression was 35.18%, the fracture area expanded, a part of dislocation appeared on the side of sample and broken cell partly also appeared on the bottom of the sample. As the compression proceeded, the fracture area spread and the cell walls fragmented and some regions became dense. The cell walls fracture without undergoing significant elastic deformation prior to fracture, which is consistent with the fluctuations of the stress-strain curve.

For **Foam II**, it can be seen that as the compression increases, the deformation appears at the top of the sample first, the cell walls become bent, and there is no significant change in other parts of the sample (as shown in **Figure 5H**).

From **Figure 5** (**K** and **I**), it can seen that there are many missing cell walls on top of the sample, and the cell walls at the bottom of the sample are more complete. When compressed, the cell walls on the top experience bending deformation first. When compression is 40%, the number of bending cells increases, the

deformation extends to the middle of the sample, but there are no cracks in cell walls, and the cell shape at the bottom is not significantly changed. The cell walls in the upper part of the sample are connected with the cell walls in the bottom part. As the height of the sample becomes lower, the width becomes larger, and the extension appears at the top of the sample because of the compression (as shown in **Figure 5I**).

Foam I: a0%, b6.32%, c15.27%, d18.43%, e35.18%, f39.70% compression
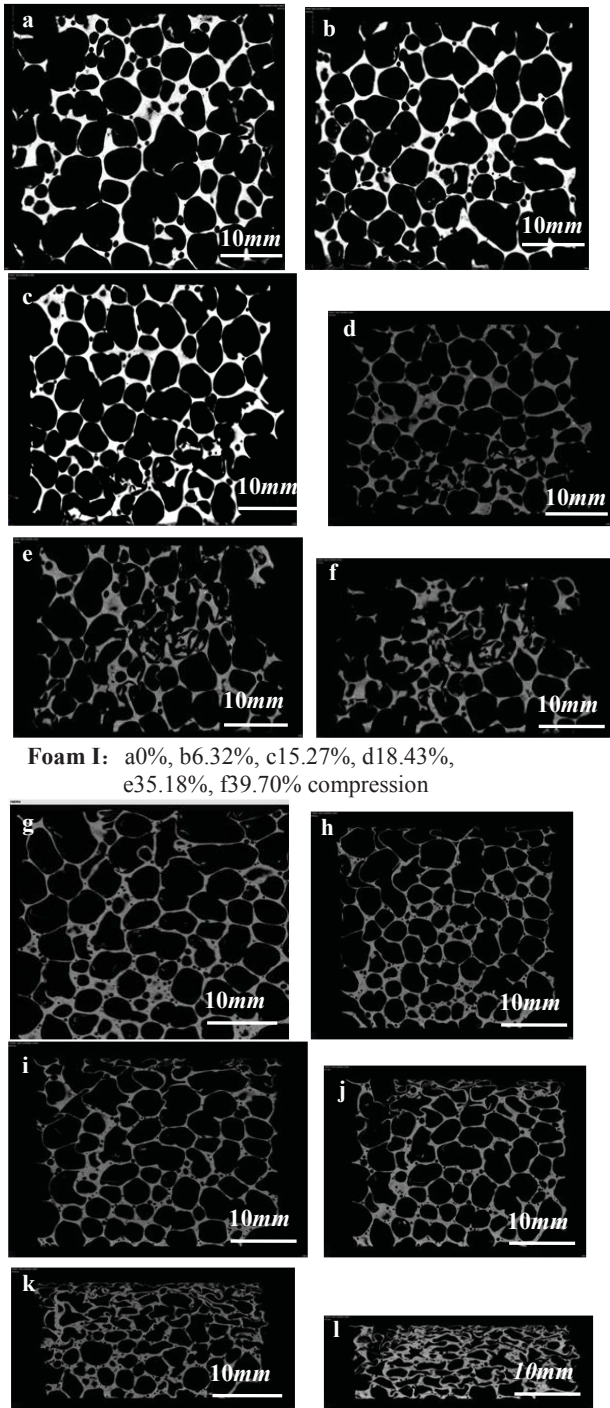
Foam II: g 0%, h 5%, i10%, j 20%, k 40%, l 60% compression
Figure 4 2D pore morphology **evolution** in difference compression
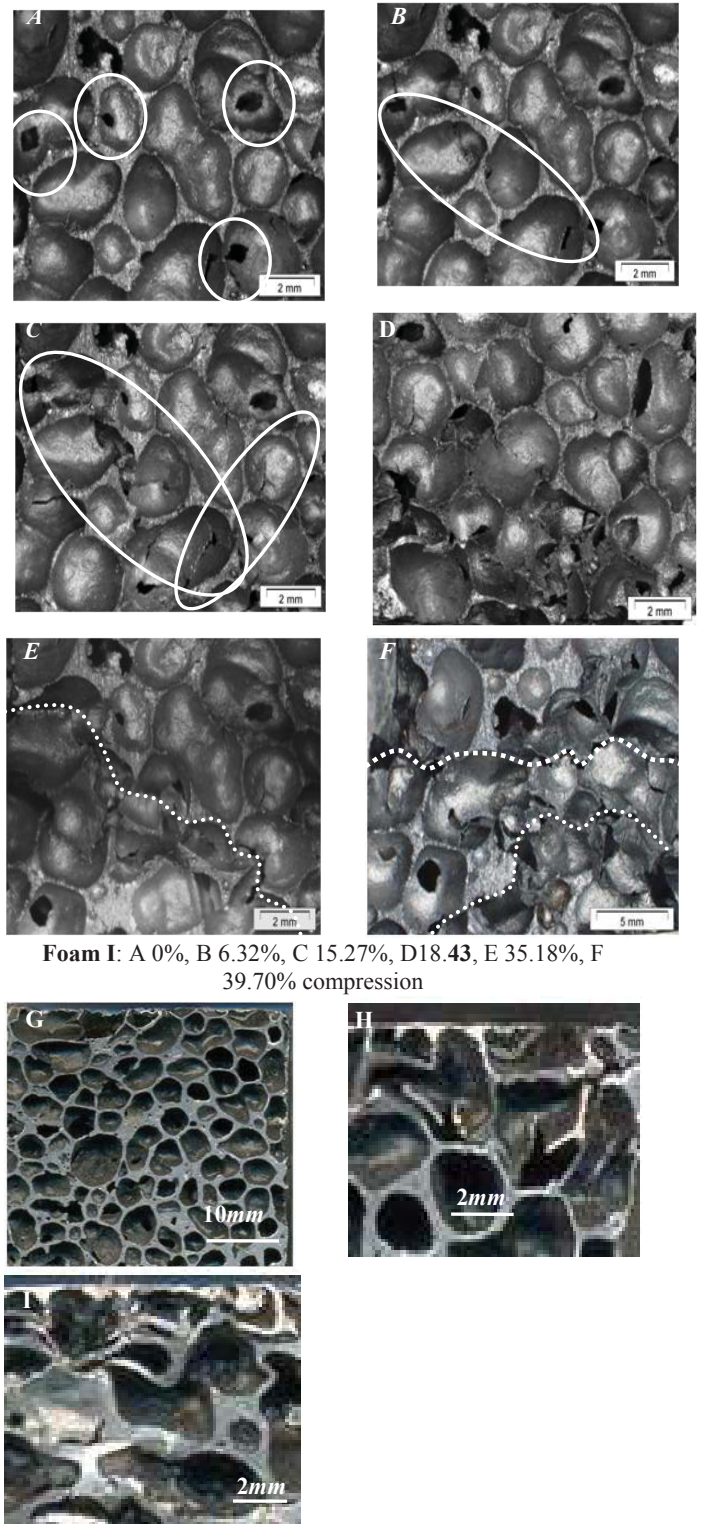
Foam I: A 0%, B 6.32%, C 15.27%, D18.**43**, E 35.18%, F 39.70% compression

Foam II: G 0%, H10%, I40% compression
Figure 5 Microstructure of the aluminum foams specimen in difference compression stage

438

Conclusions

To analyze pore morphology change of every section of aluminum foam in the course of compression by X-ray CT, can obtain results as follows: there are a large number of cells with ranges widely dispersed in size, cell size focus in 0-6.0m。 As the compression increases, larger size cells were compressed and shrunk first, the percent of small size cell increases, and the large cells disappear gradually, until the aluminum foam is compacted. Cell destruction is related with its location and geometry.

Evolution of cell morphology is closely related to the structure of cell wall and the characteristic of the matrix materials. For Al-Si alloy foam, since the matrix materials are of poor scalability, cell walls show brittle fracture in the compression process. Cell wall defect is the direct cause of pushing forward cell wall breakage. Breaking is first produced in a defective area, as the pressure increases, the crack continues to expand and deepen, and ultimately forms many fracture zones, until the whole sample is compacted and crushed. For Al-Mg alloy foam, since the matrix materials is of good ductility, bending deformation first occurs in the area of defective parts of cell wall and extends to other parts constantly, until the whole sample is compacted.

Acknowledgement

Reference

[1] MUKHRJEE M, RAMAMURTY U, GARCIA-MORENO F, BANHART J. The effect of cooling rate on the structure and properties of closed-cell aluminum foams. Acta Mater, 58 : 5031-5042(2010)

[2] RACK A, HELWIG H-M, BUTOW A, BANHART J. Early pore formation in aluminum foams studied by synchrotron-based micro-tomography and 3-D image analysis. Acta Mater., 57:4809-4821(2009)

[3] YAO Guang-chun, LIU Yi-han. Advanced property technology of materials. (Shenyang, Northeastern University Press, 2007) P.70-88.

[4] JAE U C, SOON J H, SANG K, CHONGDU C. Impact fracture behavior at the material of aluminum foam. Materials Science and Engineering A. 539:250-258(2012)

[5] JEON I, KATOU K, SONODA T. Cell wall mechanical properties of closes-cell Al foam. Mechanics of Materials, 41: 60-73(2009)

[6] JEON I, ASAHINA T, KANG K, IM S, LU Ti. Finite element simulation of the plastic collapse of closed-cell aluminum foams with X-ray computed tomography. Mechanics of Materials, 42:227-236 (2010)

[7] ASHBY MF, EVANS A, FLECK NA. Metal Foams-a design guide, Butterworth-, Boston, (2000)

[8] ZUO Xiao-qing, Kennedy A R, Wang Yong-sheng. Fabrication and compressive properties of Al foam with fine cell structure. Rare Metal Materials and Engineering, 38, (Suppl), 3:254-258(2009)

[9] MUKHRJEE M, GARCIA-MORENO F, BANHART J. Defect generation during solidification of aluminum foams. Scripta Materialia, 63:235-238(2010)

[10] ZHANG C J, FENG Y, ZHANG X B. Mechanical properties and energy absorption properties of aluminum foam-filled square tubes. Transactions of Nonferrous Metals Society of China, 20:1380-1386 (2010)

[11] TABIBIAN S, CHARKALUK E, CONSTANTINESCU A. Behavior, damage and fatigue life assessment of lost foam casting aluminum alloys under thermo-mechanical fatigue conditions. Procedia Engineering, 2:1145-1154 (2010)

[12] SEITZBERGER M, RAMMERSTORFER F G, GRADINGER R. Experimental Studies on the Quasi-static Axial Crushing of Steel Columns Filled with Aluminum Foam. International Journal of Solids and Structures, 37:4125-4147(2000)

[13] DE GIORGI M, CAROFALO A, DATTOMA V. Aluminum foams structure modeling. Computers & Structures, 88:25-35(2010)

[14] YU Ying-hua, YANG Zhi, LIANG Bing. Finite element simulation of foamed aluminum compression behavior, 27(7):317-320 (2010)

[15] SAADATFAR M, GARCIA-MORENO F, HUTZLER S. Imaging of metallic foams using X-ray micro-CT. Colloids and Surfaces A: Physicochemical and Engineering Aspects, 344:107-112(2009)

[16] YANG Fu-jun, TANG Zhao-chen, ZHU Li, at al. Experimental study on cellular structure statistical analysis and uniaxial deformation behavior of closed-cell aluminum foam. Journal of Southeast University (Natural Science Edition), 39(2):250-254(2009)

[17] WEI Li, SINKA Csaba, LAWES Simon, HAN Tao. Compressive .behavior of aluminum foams prepared by powder metallurgy method. Mechatronics and Applied Mechanics,156-157:600-603(2012)

[18] WEI Li, SINKA Csaba, CHE Lida, Statistical analysis of pore structure and compression behavior of Al-Si foams. Int. J. Modelling, Identification and Control(To be publishing)